Building Designed Granular Towers One Drop at a Time

Julien Chopin* and Arshad Kudrolli†

Department of Physics, Clark University, Worcester, Massachusetts 01610, USA

(Received 27 August 2011; published 9 November 2011)

A dense granular suspension dripping on an imbibing surface is observed to give rise to slender mechanically stable structures that we call granular towers. Successive drops of grain-liquid mixtures are shown to solidify rapidly upon contact with a liquid absorbing substrate. A balance of excess liquid flux and drainage rate is found to capture the typical growth and height of the towers. The tower width is captured by the Weber number, which gives the relative importance of inertia and capillary forces. Various symmetric, smooth, corrugated, zigzag, and chiral structures are observed by varying the impact velocity and the flux rate from droplet to jetting regime.

DOI: 10.1103/PhysRevLett.107.208304 PACS numbers: 83.80.Hj, 47.20.Hw, 45.70.Qj

From splashing to bouncing and atomization, drop impact attracts attention due to the beauty of the shapes resulting from a subtle interplay between inertia, surface tension, viscosity, and the substrate [1–4]. On granular substrates, impact can create craters [5–7] that can be used to infer properties such as impact velocity and drop size [8,9]. Here, we report observation of slender stable structures—which we call granular towers—that can be created drop by drop by dripping a dense suspension of grains on a liquid absorbing surface such as blotting paper or a dry granular bed. As a growth process, the tower structures appear analogous to frozen lava flows, icicles, and stalagmites found in nature, and microfabricated structures with ceramic ink jet printing [10–13], but have a different physical origin.

If a dense suspension of grains mixed with a liquid is poured on a solid substrate it can spread like an effective viscous fluid [14–16] or form a pile with an angle of repose [17] depending on the sedimentation rate and the material properties of the grains. However, an imbibing substrate can have a tremendous effect on the flow of a granular suspension because it can quickly absorb the liquid in the suspension, rapidly causing the particles in it to jam, leading to the formation of stable structures. Indeed, drip castles on a beach are made exploiting this property.

We demonstrate with high speed imaging that the excess liquid is quickly drained from the granular suspension upon impact and the structure is essentially frozen thereafter. We find that the size of the towers can be determined by balancing the excess liquid flux and the drainage through the granular tower. Increasing the rate of flux from a nozzle can lead to a transition from a droplet regime to a jetting regime. Further, the free-fall time and the density of the suspension play a significant role in determining the shape of the drop before impact, and the impact velocity is observed to control the spreading of the drop upon impact. We show that these facts can be manipulated to give rise to a rich array of delicate structures using granular suspensions.

The granular suspensions used consist of combinations of tens of micron scaled glass beads and water-glycerine liquid mixtures summarized along with the corresponding grain and liquid properties in Table I [18]. The granular suspension (GS) is prepared in a 100 mL syringe by first pouring 50 mL of liquid and then filling it with beads. The liquid surface tension is $\gamma \sim 70 \times 10^{-3}$ J $\cdot$ m^{-2}. The syringe is oriented vertically above the substrate and pushed by a stepper motor allowing us to vary the volumetric flux Q in the range 1–100 mL/min [see Fig. 1(a)]. The syringe nozzle has a 2.35 mm inner diameter and delivers drops typically $d_0 \sim 4$ mm in diameter. A moving stage driven by a second stepper motor allows us to vary the nozzle-substrate distance H in the range 10–300 mm. Depending on the flux and the rheology of the suspension, drops or a continuous thread are obtained. The dripping period T, which is the time between two successive drops and the drop volume V, depend on the pinch-off dynamics and are related to the flux rate by $T = V/Q$. T is constant at low flux rate $Q < 10$ mL/min. Unless stated otherwise, the substrate is a dry granular bed 10 mm deep with the same beads used in the suspension for simplicity of analysis. We carefully measured the volume fraction ϕ of the grains in the drop before impact [18]. Although each suspension has a specific dependence of ϕ on Q, ϕ is more or less constant for $Q > 0.5$ mL/min. Using GS-1, ϕ can be set to a low value ($\phi = 55\% \pm 0.3$) at high Q or a high value ($\phi \sim 58\%$) at low Q. In our experiment, the control parameters include the volumetric flux Q and the distance nozzle-substrate H. The shape of the drop before impact depends on H and ϕ. Further, the suspension properties have been varied using two sizes of glass beads and by increasing the viscosity of the liquid.

Figures 1(b)–1(f) show images of structures obtained after dripping GS-1 on various substrates under otherwise similar conditions. Using an impermeable smooth or rough substrate, the suspension spreads uniformly like an effective viscous fluid [Figs. 1(b) and 1(c)]. However, a dramatic change occurs in the obtained structure when the

TABLE I. Glass bead and suspension properties where r is the bead size, p_c the capillary pressure, k the permeability, μ the viscosity of the interstitial fluid, ϕ the drop volume fraction before impact, and ρ the suspension density.

Label	r (μm)	p_c (kPa)	k (μm^2)	μ (mPa · s)	ϕ (%)	ρ (kg · m^{-3})
GS-1	35 ± 20	5.2	5.1	0.9	55–58	1.7×10^3
GS-2	35 ± 20	5.2	5.1	5.1	55–58	1.7×10^3
GS-3	17 ± 10	9.3	1.3	0.9	58	1.9×10^3

substrate can absorb liquid as shown on filter paper [Fig. 1(d)] and dry granular substrate [Figs. 1(e) and 1(f)]. By increasing the drip time, extremely slender and mechanically stable towers can be obtained [see Fig. 1(f)].

To elucidate the growth of a tower and the importance of drainage of liquid from the suspension soon after contact, we show in Fig. 2 a sequence of images of a structure just before and after the impact obtained with a high frame rate Phantom V5.0 camera. Just after impact, the presence of a liquid film around the beads leads to a specular reflection of light as evidenced by the bright spot indicated by the arrow. As the liquid drains, the reflection appears more diffused, indicating that water has drained from the just-impacted drop (similar to the preimpact image.) The time scale here is of order tens of milliseconds for GS-1 and increases with the tower height.

To gain insight into the internal structure of the tower, an x-ray computed tomography revealed that the structure is almost fully saturated with liquid (and very few air pockets were detected) [18]. Because no voids were found and the

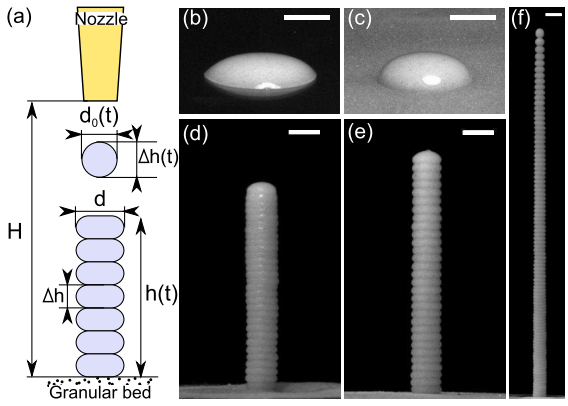

FIG. 1 (color online). (a) Schematics of the experiment showing a syringe nozzle, a granular tower of height $h(t)$, and a falling drop of thickness $\Delta h_0(t)$ and diameter $d_0(t)$. The drop diameter and thickness after impact are d and Δh, respectively, the distance nozzle-substrate is H. (b)–(e) Images after dripping GS-1 ($H = 150$ mm, $T \sim 300$ ms, $Q = 4.77$ mL/min) on various substrates: (b) glass slide, (c) glass slide coated with a layer of glass beads of 70 μm diameter, (d) coffee filter paper (Melita, No. 2), (e) 10 mm deep bed of glass beads. (f) Very slender and mechanically stable tower can be obtained by dripping the GS for a longer time interval. The scale bar is 5 mm.

particles look randomly distributed inside the structure, the solid volume fraction $\phi^\star$ of the tower is then assumed to be 63%. Therefore, we conclude that the surface of the granular tower corresponds to an air-liquid interface with menisci of order r due the presence of glass beads. A lower Laplace pressure $p_c \sim 2\gamma/r \sim 5$–$10$ kPa thus develops in the interstitial liquid which leads to a net cohesive force between the particles. This force along with friction holds the structure mechanically together.

It is convenient to express the liquid volume that drains as a function of ϕ and $\phi^\star$. Introducing V, V_G, and V_E as the volume of the drop before impact, the volume of grains, and the excess volume of liquid, respectively, we have $\phi = V_G/V$ and $\phi^\star = V_G/(V - V_E)$. The fraction of liquid to be drained $\delta w = V_E/V$ is then equal to $(\phi^\star - \phi)/\phi^\star$. From our measurements of ϕ [18], we get $\delta w = 5\%$–15%.

Next, we illustrate the effect of the flux on the morphology of the structure obtained varying the flux from the droplet regime to a continuous jet regime. Figure 3(a) shows a set of towers obtained by varying Q in the range 1–100 mL/min with GS-3 and $H = 150$ mm. The dripping time has been adjusted so that the volume of the towers is the same. Various symmetric tower shapes are observed except at the highest flux in addition to an overall decrease in height with Q. For $Q < 3$ mL/min, towers with essentially a symmetric corrugated surface from the substrate up to the tip are observed. As Q increases, only the lower part of the tower exhibits a regular pattern whereas the upper part is smoother and wider. Further, by increasing the flux and the viscosity of the suspension to be in the continuous jet regime [Fig. 3(g)], a tower structure is not observed. Instead, a suspension sheet spirals around giving rise to a chiral pagoda domelike structure [18].

Because the flux is held constant in these experiments, the growth of the height can be related easily to the cross section, and therefore we plot the temporal evolution of height of the structures [see Fig. 3(h)] and use it for further analysis. An important feature of these curves is the linear increase of the tower height h [indicated by gray (red) lines] that is present initially for all volumetric fluxes and indicates surprisingly that the growth rate is independent of h in this regime. Therefore, as long as the tower is smaller than a crossover height h_X, all the drops are jammed before

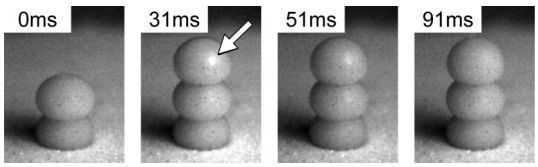

FIG. 2. Sequence of drop impact and subsequent drainage (GS-1, $Q = 4.77$ mL/min, $H = 20$ mm). The bright spot (see arrow) indicates the presence of liquid film which disappears due to the liquid drainage. The tower width is 5 mm.

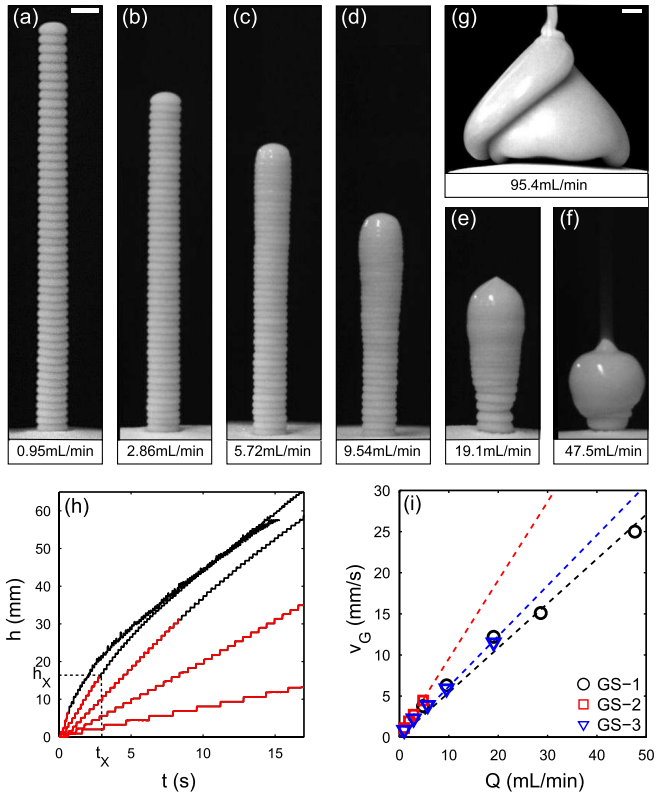

FIG. 3 (color online). (a)–(g) Structures built using GS-3 by increasing Q, and two μ 1 mPa · s (a)–(f) and 5.1 mPa · s (g). (h) Temporal evolution of the tower height h for an increasing Q using GS-3. h increases linearly for $t < t_X$ up to a height h_X [gray (red) lines]. (i) The growth velocity v_G calculated from a linear fit is proportional to Q. Using Eq. (1), linear fits (solid and dashed lines) gives access to the diameter of the tower: 6.2 mm (GS-1), 4.7 mm (GS-2). and 5.9 mm (GS-3).

the impact of the next drop and are deformed in exactly the same way independently of the tower height. We then define a growth velocity $v_G = \Delta h/T$, where $\Delta h = (V - V_E)/s$ is the drop thickness which leads to

$$v_G = \frac{\phi}{\phi^\star}\frac{Q}{s}, \tag{1}$$

where $s = \pi d^2/4$ is the horizontal cross section area. The proportionality of the velocity growth with the volumetric flux for GS-1, GS-2, and GS-3 is shown in Fig. 3(i) and indicates that the drop area is essentially independent of Q.

In order to understand what sets the crossover height h_X and the crossover time t_X, we plot $h(t)$ in Fig. 4(a) for GS-1 ($Q = 9.54$ mL/min, $v_G = 6.31$ mm · s^{-1}), GS-2 (4.75 mL/min, 4.46 mm · s^{-1}), and GS-3 (9.54 mL/min, 5.95 mm · s^{-1}), keeping the growth velocity approximately the same in each case by varying the volumetric flux. The deviation from a linear growth appears earlier when d is decreased or when μ is increased. In Fig. 4(b), the crossover height h_X indeed shows a strong variation with the volumetric flux. Our interpretation of

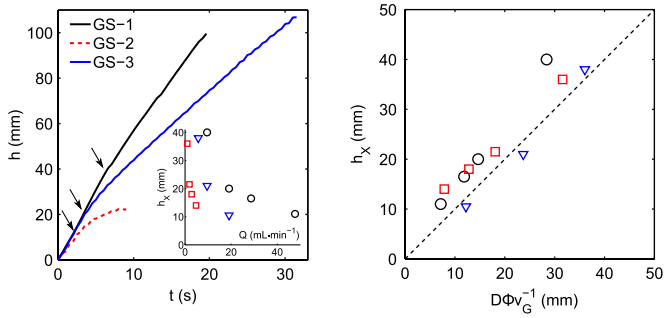

FIG. 4 (color online). (a) Tower height h versus t. The growth velocity is roughly the same for the three cases 6.31 mm · s^{-1} (GS-1), 4.46 mm · s^{-1} (GS-2), 5.95 mm · s^{-1} (GS-3), whereas the crossover length h_X decreases significantly for each case (see arrows). Inset: Corresponding h_X versus Q (same symbols as Fig. 3). (b) Crossover height h_X as a function of $D\Phi v_G^{-1}$ [see Eq. (2)]. The data collapse reasonably well on the line as captured by our model.

this behavior relies on the comparison of the flux of liquid by imbibition with the incoming flux we impose with the syringe. As long as the imbibition is fast enough, the growth is linear with time. The onset of the deviation from linearity appears when the incoming flux of water is equal to the flux set by the imbibition process down in the substrate which can be modeled by a Washburn-Lucas law [19]. We then write the maximum liquid flux $j_D = Dh^{-1}$, where $D = p_c k/\mu$ and p_c the capillary pressure. Using the expressions of δw and v_G, the flux of excess liquid $j_L = V_E/(sT)$ is equal to $v_G(\phi^\star - \phi)/\phi$. The condition $j_L = j_D$ leads to a determination of the crossover height h_X:

$$h_X = D\Phi\frac{1}{v_G}, \tag{2}$$

where $\Phi = \frac{\phi}{\phi^\star - \phi}$. Recalling that $h_X = v_G t_X$, the crossover time is $t_X = D\Phi/v_G^2$. This leads to $h_X = \sqrt{D\Phi t_X}$. Figure 4(b) shows the evolution of the crossover height h_X as a function of $D\Phi/v_G$. All the data collapse quite well on a line with slope 1, indicating that our simple model is sufficient to provide a quantitative understanding of the growth of a tower. Furthermore, good agreement also shows that the role of evaporation and drainage by gravity is negligible in our experiments.

Next, we examine the precise shape of the tower where two main factors involved are the preimpact aspect ratio $\Delta h_0(t)/d_0(t)$ of the drop and the impact velocity v, both of which can be varied by adjusting H. We have recorded the free fall of a GS-1 drop with a high frame rate camera and measured the temporal evolution of its aspect ratio for $\phi = 55\%$ and $\phi \sim 58\%$ [see Fig. 5(a)]. For low ϕ, the drop is initially oblate and relaxes towards an almost spherical shape after a typical time $\tau_r \sim 30$ ms. Just after pinch-off, no capillary waves were observed, indicating that inertial effects are negligible compared to viscous or

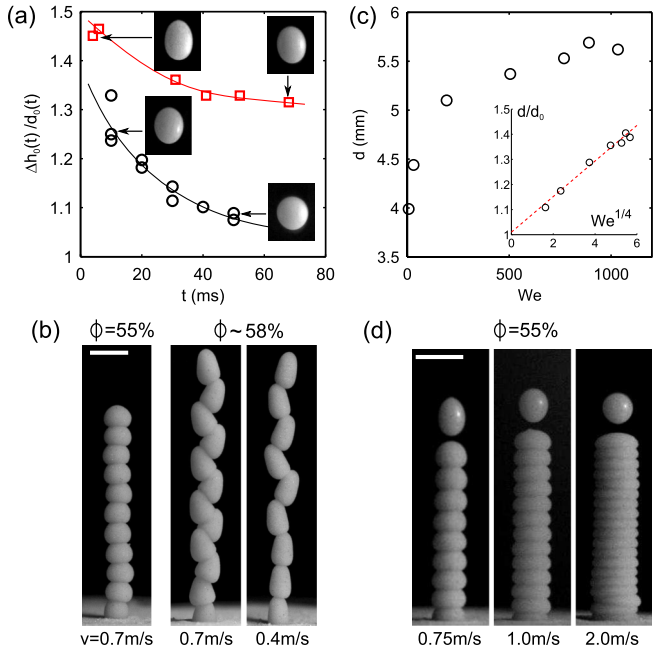

FIG. 5 (color online). (a) Temporal evolution of the aspect ratio $\Delta h_0(t)/d_0(t)$ of a GS-1 drop during its free fall. At $t = 0$ s, the drop detaches from the nozzle. At low volume fraction ($\phi = 55\%$, $Q = 4.77$ mL/min), the shape relaxes towards a sphere (○). At higher volume fraction ($\phi \sim 58\%$, $Q = 0.48$ mL/min), the relaxation is greatly slowed down (□). (b) Tower morphologies for low (55%) and high ($\sim 58\%$) volume fraction in a low impact velocity regime. (c) Evolution of the drop diameter d after impact with the Weber number $\mathrm{We} = 2\rho v^2 d_0/\gamma$ using GS-1. Inset: The nondimensional diameter d/d_0 scales reasonably well with $\mathrm{We}^{1/4}$. (d) Tower morphology varies with the impact velocity v. The images are taken just before impact and show the shape of the falling drop. The scale bar is 5 mm.

frictional losses [20]. Modeling the granular suspension as an effective viscous fluid with viscosity μ_{eff}, τ_r may be given by a balance of surface tension and viscous losses yielding $\tau_r \sim \mu_{\mathrm{eff}} d/\gamma$. From this scaling, we have estimated $\mu_{\mathrm{eff}} \sim 500$ mPa · s, which is compatible with previous estimates of granular suspensions [14,16]. However at higher ϕ, τ_r is much larger and the drop appears to remain jammed in an oblate shape. Therefore, frictional effects might be important and the modeling GS by a simple effective viscosity is likely to break down.

We observe that for small velocity impact, impacted drops with low ϕ are almost spherical [Fig. 5(b)]. At higher volume fraction ($\phi \sim 58\%$), the impacted drops remain elongated keeping memory of their shape upon impact. The vertical orientation is less stable so that the drop can exhibit a tilt in the opposite direction from one drop to the other, resulting in a zigzag shaped tower.

However, the deformation of the drop can be affected increasing the impact velocity. We have measured the drop diameter after impact d by varying H in the range 3–300 mm for GS-1. Figure 5(c) shows the evolution of d (GS-1, $Q = 2.86$ mL/min, $\phi = 55\%$) with Weber number $\mathrm{We} = 2\rho v^2 d_0/\gamma$, where $\rho = 1.7 \times 10^3$ kg · m^{-3} is GS density and d_0 the drop diameter just after impact. The Weber number quantifies the relative importance of inertia with capillary forces. We measured the impact velocity by recording the drop fall operating the Phantom camera at 2100 frames per second. We ignored the first drop impact on the granular bed as the physics might be different due to crater formation and therefore consider the second drop. We found that the nondimensional diameter d/d_0 scales reasonably well with $\mathrm{We}^{1/4}$ as shown in previous studies with other systems [2,7]. For $\mathrm{We} < 100$, the drop does not have sufficient time to be spherical but, interestingly, the scaling given above is not highly sensitive to its aspect ratio. This behavior enables us to build towers with fine or coarse corrugations by adjusting the velocity impact [see Fig. 5(d)].

In conclusion, dripping of a dense granular suspension on a granular substrate is observed to give rise to a rich array of delicate mechanically stable granular tower structures. Besides applications in surface patterning, this tower building technique may be a new and easy way to probe the rheological properties of dense granular suspensions where the shape of the tower is the response and the impact velocity the forcing parameter.

*jchopin@clarku.edu
†akudrolli@clarku.edu

[1] A. Worthington, Proc. R. Soc. London **25**, 261 (1876).
[2] D. Richard and D. Quéré, Europhys. Lett. **50**, 769 (2000).
[3] J. Eggers, Rev. Mod. Phys. **69**, 865 (1997).
[4] A. L. Yarin, Annu. Rev. Fluid Mech. **38**, 159 (2006).
[5] J. Uehara, M. Ambroso, R. Ojha, and D. Durian, Phys. Rev. Lett. **90**, 194301 (2003).
[6] S. Deboeuf, P. Gondret, and M. Rabaud, Phys. Rev. E **79**, 041306 (2009).
[7] H. Katsuragi, Phys. Rev. Lett. **104**, 218001 (2010).
[8] W. Bentley, Mon. Weather Rev. **32**, 450 (1904).
[9] R. Metz, J. Sediment. Res. **51**, 265 (1981).
[10] R. W. Griffiths, Annu. Rev. Fluid Mech. **32**, 477 (2000).
[11] A. S. H. Chen and S. W. Morris, Phys. Rev. E **83**, 026307 (2011).
[12] M. B. Short, J. C. Baygents, J. W. Beck, D. A. Stone, I. R. S. Toomey, and R. E. Goldstein, Phys. Rev. Lett. **94**, 018501 (2005).
[13] X. Zhao, J. R. G. Evans, M. J. Edirisinghe, and J. H. Song, J. Mater. Sci. **37**, 1987 (2002).
[14] I. Zarraga, D. Hill, and D. Leighton, J. Rheol. **44**, 185 (2000).
[15] J. Zhou, B. Dupuy, A. Bertozzi, and A. Hosoi, Phys. Rev. Lett. **94**, 117803 (2005).

[16] C. Bonnoit, T. Darnige, E. Clément, and A. Lindner, J. Rheol. **54**, 65 (2010).
[17] A. Samadani and A. Kudrolli, Phys. Rev. E **64**, 051301 (2001).
[18] See Supplemental Material at http://link.aps.org/supplemental/10.1103/PhysRevLett.107.208304 for movies of tower formation, methods used to obtain material properties, and x-ray internal imaging of the structure.
[19] E. W. Washburn, Phys. Rev. **17**, 273 (1921).
[20] H. Lamb, *Hydrodynamics* (Dover, New York, 1945).